Hindawi
Shock and Vibration
Volume 2018, Article ID 8439321, 18 pages
https://doi.org/10.1155/2018/8439321

Research Article

An Experimental Investigation of Unbonded Laminated Elastomeric Bearings and the Seismic Evaluations of Highway Bridges with Tested Bearing Components

Gang Wu,[1] **Kehai Wang**,[1,2] **Guanya Lu**,[1] **and Panpan Zhang**[2]

[1]*School of Transportation, Southeast University, Nanjing, Jiangsu, China*
[2]*Research Institute of Highway, Ministry of Transport, Beijing, China*

Correspondence should be addressed to Kehai Wang; kh.wang@rioh.cn

Received 20 June 2017; Revised 20 November 2017; Accepted 17 December 2017; Published 16 January 2018

Academic Editor: Nerio Tullini

This paper presents an experimental program performed to investigate the behavioral characteristics of unbonded steel-reinforced laminated elastomeric bearings (U-SLEBs), which have been widely used for highway bridges in China. The influences on the friction behaviors, stiffness, and energy dissipations of the different parameters, such as compressive stresses, loading rates, and rubber material, were discussed. The responses of the U-SLEBs were compared with those of the bonded steel-reinforced laminated elastomeric bearings (B-SLEBs). Then, effective analytical models were developed, which considered the mechanical degradation of the U-SLEBs and simulated the realistic behaviors of the B-SLEBs. The seismic responses of a multispan continuous bridge with tested bearing components were also evaluated. The results showed that the mechanical properties of the U-SLEBs tended to degrade due to friction sliding. However, the degrees of the decrease were found to be dependent on the influencing parameters. Meanwhile, the B-SLEBs exhibited stiffening behaviors that led to tearing under large displacement demands. The bridges using U-SLEBs were found to suffer less damage due to the reliable sliding behavior of U-SLEBs. It is recommended that shear keys, which are reasonably designed in the transverse direction, be constructed in order to achieve better seismic performance.

1. Introduction

China is known to be an earthquake-prone country, especially in the western areas that are characterized by high seismicity. There have been many severe earthquakes during the past decade, such as the Wenchuan earthquake in 2008 with a magnitude of 8.0 Ms and the Yushu earthquake in 2010 with a magnitude of 7.1 Ms. These earthquake events resulted in different degrees of bridge damage in most of the important relief lines. The postearthquake damage investigations of the small-to-medium spanning highway bridges showed that the most typical types of seismic damage included girder movements or girder falling, sliding or unseating of laminated elastomeric bearings, shear keys failure, damage to expansion joints, and abutment cracking. Meanwhile, the piers displayed relatively low seismic damage ratios [1–4]. These types of seismic damage were quite different from those observed following the Northridge and Kobe earthquakes, where the piers underwent generally serious damage. The various parts of the bridge which sustained damage resulted in varying levels of repair costs, and the earthquake relief and postdisaster reconstruction programs were affected. As can be seen in Figure 1, the Baihua Bridge experienced a collapse due to the serious damage to its piers during the Wenchuan earthquake, and it was deemed meaningless to reinforce and reuse the damaged parts. However, Shoujiang Bridge's main damage included girder movements and bearings sliding, along with slight damage to its piers. The traffic was quickly restored through the use of reinforcements including cylindrical steel jackets and steel bridge erections [5]. Therefore, it was found that the bearings, which served as crucial components to connect the superstructures and substructures of the bridges, should be able to perform good isolations to protect the substructures.

In recent years, based on the damage investigations, the design philosophy of regarding elastomeric bearings as

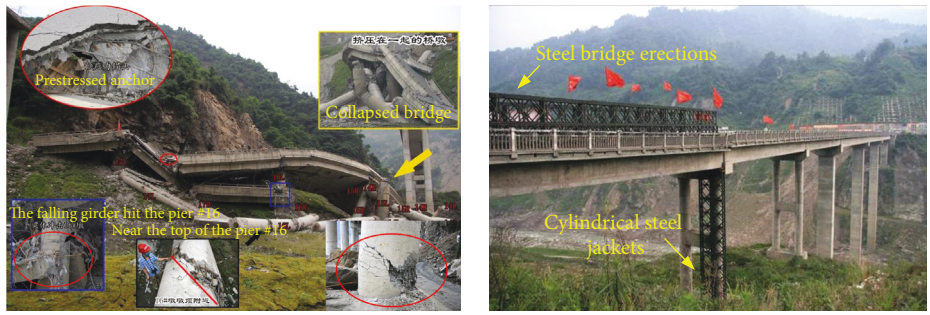

(a) (b)

Figure 1: Example of bridge damage during Wenchuan earthquake: (a) collapse of Baihua Bridge due to serious damage to its piers; (b) rapid repair of Shoujiang Bridge.

fuse elements has been gradually recognized. This design allows the bearings to exceed their server-level conditions and slide, allowing the seismic forces to be isolated and the energy to dissipate. When stating a bridge's seismic system and reinforcement strategy in the state of Illinois (USA), Tobias et al. [6] pointed out that the first tier of the three-level seismic structural redundancy is regarding the weak connections between the superstructures and substructures of bridges as "fuse elements" such as the bearings being priorities destroyed during earthquakes and the dissipation portion of the energy. Chang et al. [7] summarized the bridge seismic damage incurred during the 1999 Chichi earthquake and put forward a design concept of a functional bearing system based on a reinforcement strategy using the friction sliding characteristics of rubber bearings. Based on the earthquake seismic damage of small-to-medium span highway bridges during the 2008 Wenchuan earthquake, Wang et al. [3, 4] recommended a "multilevel fortification and hierarchical energy dissipation" philosophy, along with the principle that the damaged components and damage levels could be controlled. The damage locations were easily inspected, and the damaged components were easily repaired and replaced. Bearings should be allowed to slide during earthquake events. However, the girder falling should be prevented with effective restraining systems. Steelman et al. [8, 9] investigated the behaviors of laminated elastomeric bearings with different parameters and proposed a quasi-isolated structural design concept.

The "fused elements" design philosophy can be implemented using U-SLEBs by fully applying their predictable and controllable friction sliding characteristics. When considering the common sliding phenomenon of laminated elastomeric bearings during recent earthquake events, some researchers have focused on the friction behaviors between the bearings and the supporting surfaces. McDonald et al. [10] studied the static friction coefficient between neoprene rubber bearings and the superstructures or substructures, and their recommended value was 0.2. Steelman et al. [8, 9] concluded that the multiple cycles of large displacement demands resulted in the degradation of the friction coefficients. Therefore, the sliding distances should be considered when calculating the friction coefficients. Xiang et al. [11] and Li [12] conducted cyclic loading experiments to investigate the effects of the different influencing factors on the friction sliding of laminated elastomeric bearings, which are widely used in small-to-medium spanning highway bridges in China. However, the previous research studies have been almost exclusively based on the bearings, which had been simply anchored at the top or bottom plates. It was obvious that the bonded boundary conditions increased the stress demands on the components and changed the bearing forces and deformations [13], as well as having further effects of the friction sliding. These were hard to reflect the actual responses of the U-SLEBs. To date, only the research conducted by Konstantinidis et al. [14] has described the behavior of the U-SLEBs. This research mainly focused on the roll-off phenomenon, and no further investigations regarding the friction sliding characteristics and degradation of U-SLEBs were performed. Due to the fact that the laminated elastomeric bearings that have been used in the small-to-medium spanning highway bridges in China were usually directly placed without any anchoring at the top and bottom plates, it was necessary to study the performances of the U-SLEBs under multiple reversed cycles of large displacement demands.

The small-to-medium spanning highway bridges are the most popular type of bridges in Chinese highway networks. They are generally simply supported girder bridges or continuous girder bridges with a single span of no more than 40 m. Their superstructure is usually supported by U-SLEBs, which directly contact the girders and substructures without any anchoring. Therefore, it is useful to investigate the behavioral characteristics of U-SLEBs under multiple reversed cycles of large displacement demands and discuss the effectiveness of U-SLEBs as isolated bearings. With this in mind, this study first presented a series of laboratory tests of the U-SLEBs in order to investigate their responses under cyclic loading. The related parameters, such as compressive stress, loading rate, and rubber material, were discussed. The behavioral characteristics of the U-SLEBs were compared with the responses of the B-SLEBs. Effective analytical models of a three-span continuous bridge, which were able to simulate the realistic seismic behaviors of U-SLEBs and B-SLEBs, were then developed using the open-source, nonlinear seismic

Table 1: Test specimen characteristics.

Bearing type	Elastomer layer t (mm)	Quantity	t_r (mm)	Shim, t_s (mm)	Shaper factor	Average hardness (Shore A)	Shear modulus (MPa)	Rubber material	End plate, t_p (mm)	Quantity
Y1	7	10	70	3	13.21	62	0.95	Neoprene	—	4
Y2	7	10	70	3	13.21	64	1.01	Natural	—	3
Y3	7	10	70	3	13.21	64	1.02	Natural	20	2

Table 2: Testing matrix.

Test specimen	Bearing type	Protocol	Vertical stress (MPa)	Loading rate (mm/s)	Target ESS (%)	Boundary condition
Y1-4/30-UB	Y1	Cycle	4	30	400	Unbonded
Y1-6/30-UB	Y1	Cycle	6	30	400	Unbonded
Y1-8/30-UB	Y1	Cycle	8	30	400	Unbonded
Y1-8/45-UB	Y1	Cycle	8	45	400	Unbonded
Y2-8/3-UB	Y2	Cycle	8	3	400	Unbonded
Y2-8/30-UB	Y2	Cycle	8	30	400	Unbonded
Y2-8/45-UB	Y2	Cycle	8	45	400	Unbonded
Y3-8/30-BB	Y3	Cycle	8	30	250	Bonded
Y3-8/45-BB	Y3	Cycle	8	45	250	Bonded

Note. Unbonded boundary condition indicates that bearings do not have thick end plates, which cannot be bonded to structure. Bonded boundary condition indicates that bearings can be bonded to structure.

analysis program *OpenSees*. The seismic responses and damage mechanisms of the bridge were discussed. Finally, a rational seismic isolation design method of small-to-medium spanning highway bridges which utilized laminated elastomeric bearings was recommended.

2. Experimental Program

2.1. Description of the Test Specimens. In this research study, nine circular laminated elastomeric bearings with 370 mm diameters were tested in a laboratory. Table 1 presents the specific geometric parameters and material properties. The U-SLEBs without thick end plates which were marked as Y1 were made up of neoprene materials. The U-SLEBs without thick end plates which were marked as Y2 used natural rubber. Since all of the specimens of both type Y1 and type Y2 were not set on thick end plates (Figure 2(a)), these U-SLEBs were found to easily slip under the cyclic horizontal loading. The natural rubber bearing specimens with thick end plates (natural-B-SLEBs) were marked as Y3 (Figure 2(b)). It became obvious in the experiment that the installation and replacement of type Y3 specimens were more complex than the type Y1 and type Y2 specimens. The effects of the bonded boundary conditions on the responses of bearings were investigated by comparing the results of the type Y3 and type Y2 specimens.

All of the specimens were produced in the same batch by the Hengshui China Railway Construction Engineering Rubber Co., Ltd. In accordance with the Chinese rubber bearings test methods [15], the manufacturer conducted some tests on the supplied rubber to ensure that all the rubber properties met the specifications for the designs of highway bridge elastomeric bearings, as specified in the Chinese Standard [16]. The Rubber Shore A hardness and the shear modulus values are shown in Table 1, and the values listed in Table 1 are the mean values of the three groups' tests.

2.2. Test Setup and Procedure. This study's testing procedures were performed in the Experimental Center at the Hengshui China Railway Construction Engineering Rubber Co., Ltd. The experimental apparatus that was used is detailed in Figure 3 and included a seven-channel coordinated loading system with a maximum loading capacity of 30,000 kN. A typical testing bearing that was positioned between two steel plates is shown in Figure 3. For each of the U-SLEB specimens, there were no restraints of the horizontal movements other than friction, and the deformation of the testing protocols included the rubber shear deformations and sliding distances. The measurement of the equivalent shear strain (ESS) was used to describe the deformation. Meanwhile, for the B-SLEBs, the ESS was equal to the shear strain. Two steel rulers were fixed to the top and bottom supporting steel plates, respectively. A vertical white line was drawn on the side surfaces of each specimen in order to measure any possible relative deformations. A white gird measuring 10 cm × 10 cm, as well as the outlines of the specimens, was marked on the supporting surfaces of each steel plate in order to obtain more accurate measurements of the sliding ranges. Immediately after the completion of each test, a tool knife was used to erase rubber residue on the supporting surfaces of the steel plates, and the surfaces were scrubbed clean. The next test was performed after the steel plate surfaces had cooled in order to ensure the same contact friction conditions.

The parameters for each of this study's tests are summarized in the testing matrix laid out in Table 2. First, the vertical compressive stress applied by the vertical actuators

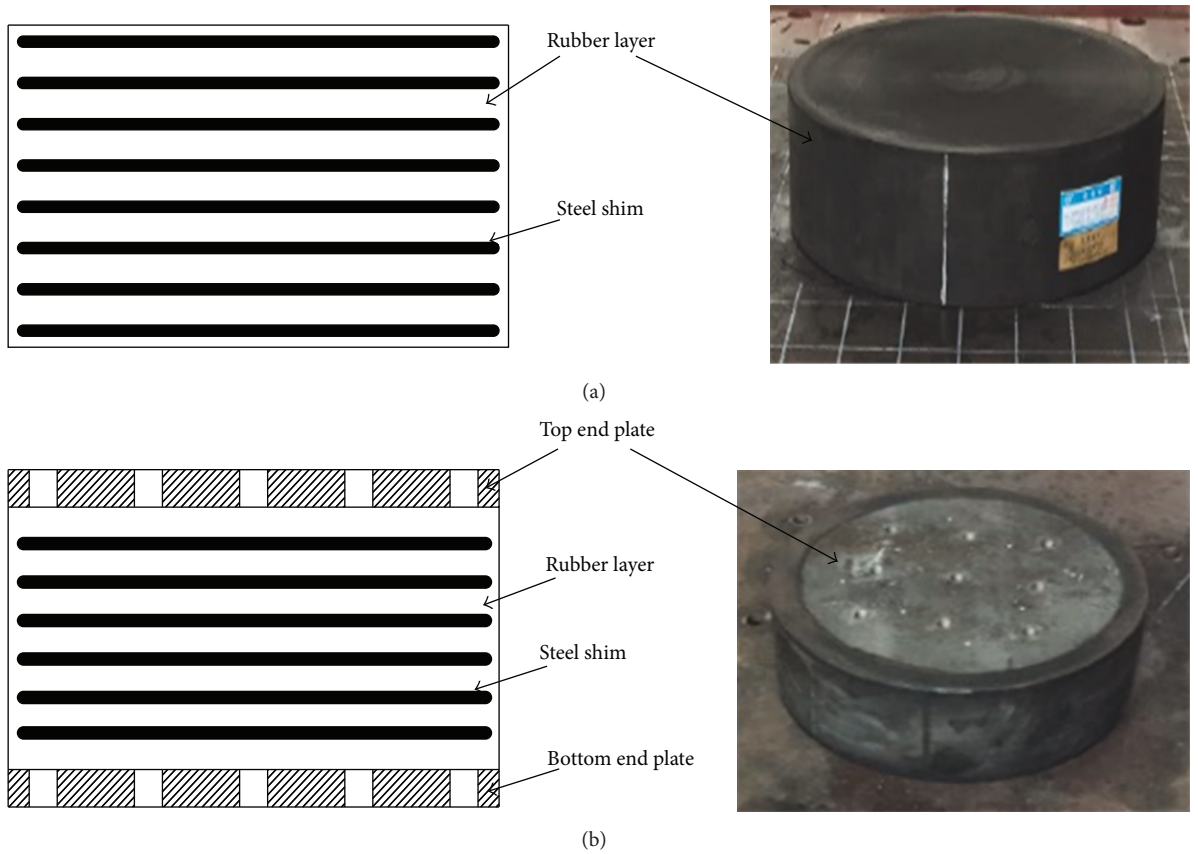

Figure 2: Sketch of testing specimens: (a) bearing type Y1/Y2; (b) bearing type Y3.

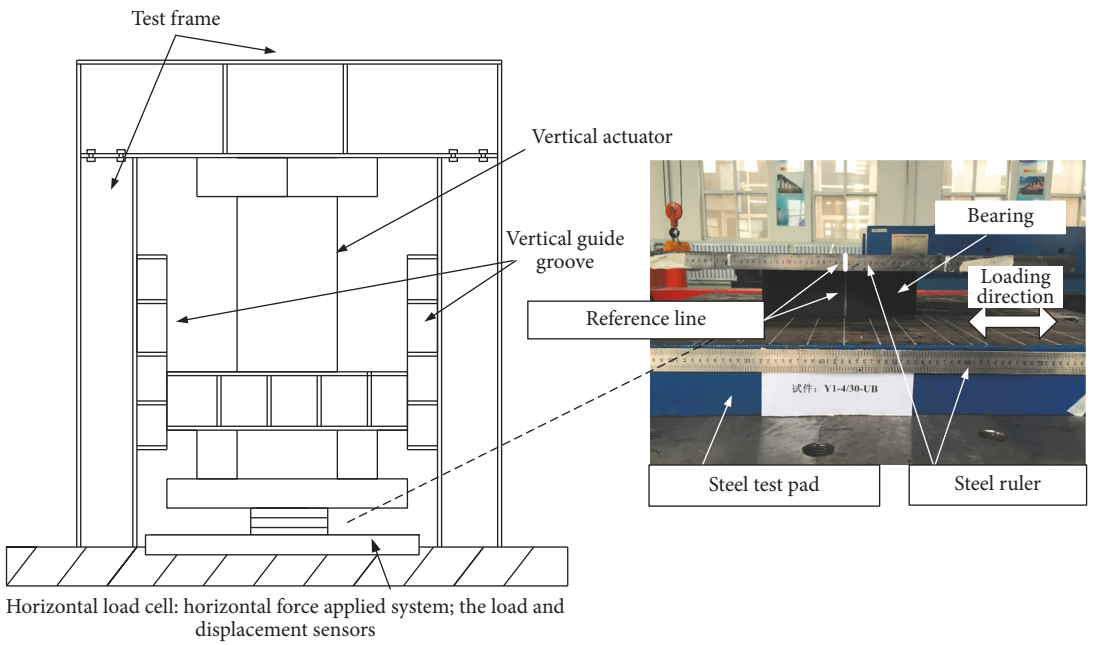

Figure 3: Testing setup.

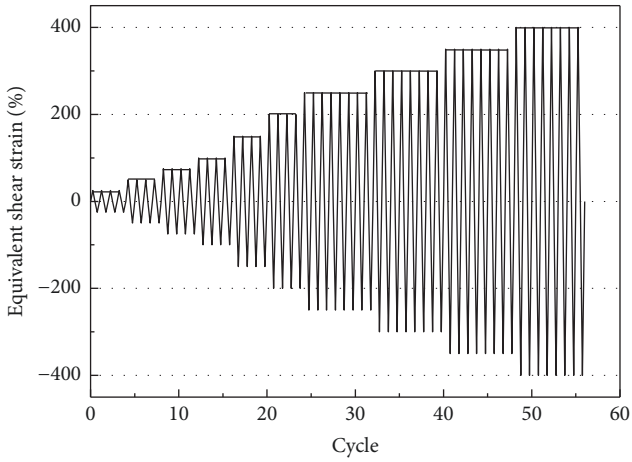

Figure 4: Cyclic testing protocol.

was maintained at a constant value. Then, cyclic horizontal displacement was imposed on the bottom supporting steel plates by horizontal actuators. The measurement of the equivalent shear strain (ESS), which is the ratio of the loading displacement to the thickness of the rubber layer t_r, was performed. A target of 400% ESS was determined for the testing program. The testing protocol shown in Figure 4 was carried out in turn according to ESS, of which the levels were as follows: 25% (4) → 50% (4) → 75% (4) → 100% (4) → 150% (4) → 200% (4) → 250% (8) → 300% (8) → 350% (8) → 400% (8), where the values in brackets represent the reversed cycles per level. Each level conducted four reversed cycles when the ESS was less than 250% and increased to eight cycles after reaching 250% ESS in order to accurately analyze the bearings' performance degradation under multiple cycles of the large displacement demands.

3. Test Results and Discussion

3.1. Responses of the U-SLEBs and B-SLEBs. The laminated elastomeric bearings with bonded and unbonded boundary conditions exhibited significantly different responses under the same loading conditions. The horizontal force-displacement hysteresis curves of the type Y2 and type Y3 specimens are provided in Figure 5 for the purpose of illustrating the key aspects of their behaviors.

The hysteresis responses of the type Y2 specimens are presented in Figures 5(a)–5(c). The red curves represent the envelope curves. The deformation of the U-SLEBs was divided into three states during the testing procedures: pure elastic shear strain of rubber layer, roll-off at the top and bottom surfaces of the bearing, and obvious friction sliding. A bearing roll-over (without sliding) described by Konstantinidis et al. [14] was not observed. For the ESS < 75%, only the pure elastic shear strain was found to exist in the rubber layer, and the bearings exhibited near linear responses. When the ESS reached 75%, a roll-off at the top and bottom surfaces of the bearings was observed due to the unbonded boundary. The shear area decreased due to roll-off and led the bearings' horizontal equivalent stiffness to degrade slightly. As can be seen in Figures 5(a)–5(c), it was observed that the type Y2 bearings began to slip at a range between 100 and 150% ESS, as indicated by the triangle markers. Also, the horizontal equivalent stiffness of the bearings declined at approximately 20%. After reaching 250% ESS, the bearings incurred visible sliding, as shown in Figure 6. The sliding distance of the specimen Y2-8/30-UB was approximately 110 mm at 250% ESS. At the same time, it was found that the horizontal force of all the type Y2 bearings had obviously decreased with the loading rate, as illustrated in Figures 5(a)–5(c). The horizontal force of specimen Y2-8/45-UB declined at approximately 30%. With the continued increase in ESS, all of the bearings were observed to exhibit stable hysteretic responses under the high shear strain. This suggested that the friction behavior between the bearings and both of the supporting steel plates basically had become stable. Generally speaking, all of the type Y2 specimens exhibited stable hysteretic performances. Although the horizontal equivalent stiffness and force displayed certain reductions, these were found to be not serious enough to lead to bearing failures, and no rubber tearing was found on the surfaces of any of the specimens during the testing procedures. Therefore, the level of sliding depended on the size of the top and bottom supporting surfaces. Provided that the U-SLEBs did not slide out of the top and bottom supporting surfaces, the bearings were able to play a strong role in isolation.

Due to the fact that the force demands of the substructure and the shear deformation of the bearings were determined by the friction characteristics between the U-SLEBs and the supporting surfaces, the first focus of this study was to determine the sliding friction coefficient of all of the U-SLEBs specimens. As detailed in the above discussion, all of the specimens started to slide at a range between 100 and 150% ESS, with the initial friction coefficient ranging between 0.09 and 0.24. Figure 7 shows that the sliding friction coefficient decreased significantly with the accumulation of the ESS. For example, the sliding friction coefficient of specimen Y2-8/30-UB was reduced by 54.4%. As can be seen in the figure, it also was observed that the sliding friction coefficient increased with the loading rate, while it decreased with the compressive stress. The dashed line represents a sliding friction coefficient of 0.1 for the steel plate supporting surfaces as specified in the Chinese code [17], which clearly underestimated the actual resistance to slipping between the rubber bearings and steel supporting plate.

Figure 5(d) shows the representative hysteresis responses of the type Y3 specimens. The red solid line represents a typical hysteretic loop under a fully reversed cyclic loading, which could be divided into three portions as follows [18]: the A-B portion describes the degeneration of the unloading; the B-C portion is an approximately constant stiffness stage; and the C-A portion is the stiffening stage of the loading. For the ESS ranging from 75 to 100%, the hysteretic loop was approximately elliptical, and the ratio between the displacement corresponding to the stiffening point and each of the cyclic loading target displacements was close to 1, which implied that stiffening behavior was still not obvious. After reaching 150% ESS, the hysteretic loop

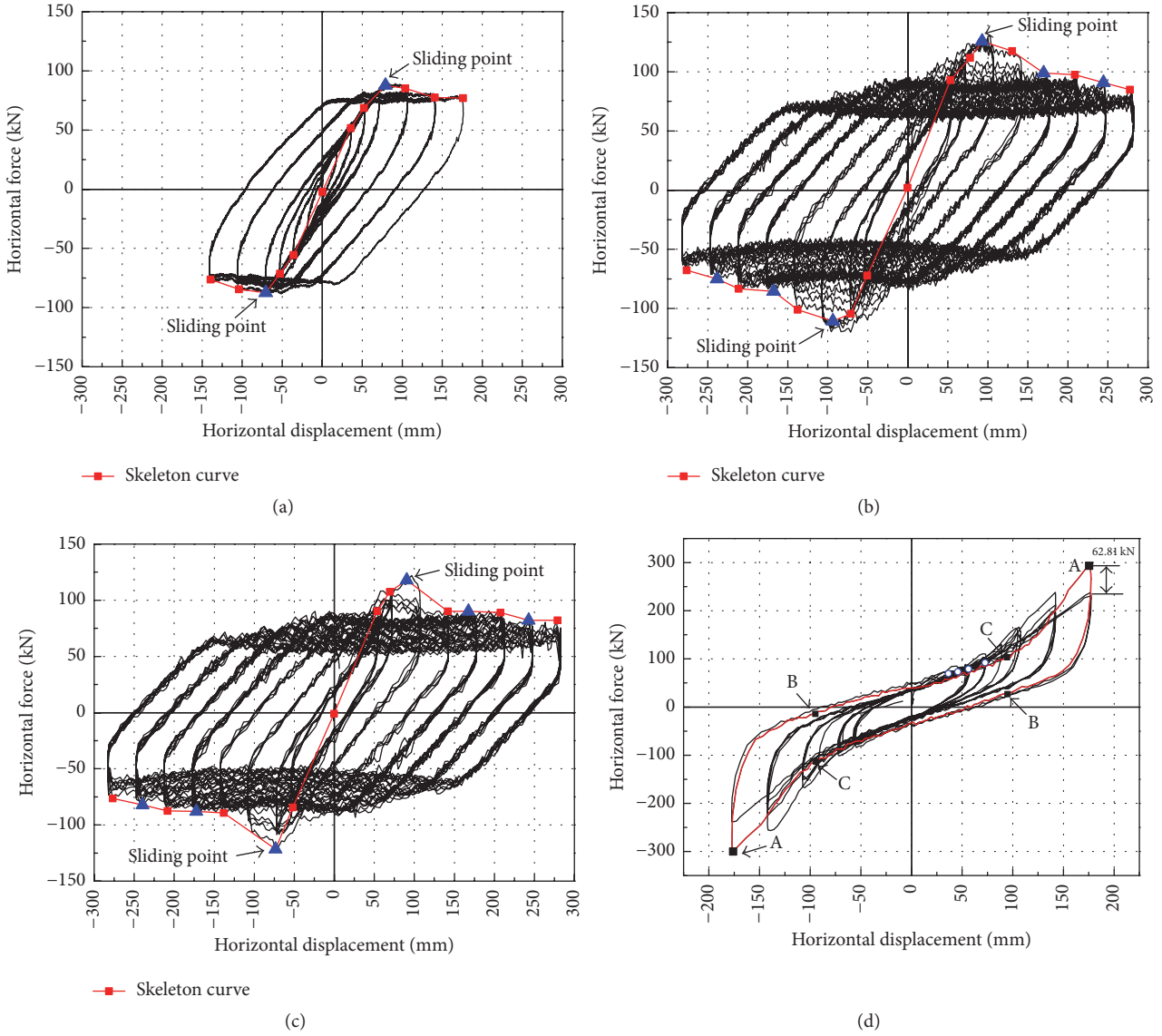

Figure 5: Force versus displacement results for the cyclic tests: (a) Y2-8/3-UB; (b) Y2-8/30-UB; (c) Y2-8/45-UB; (d) Y3-8/45-BB.

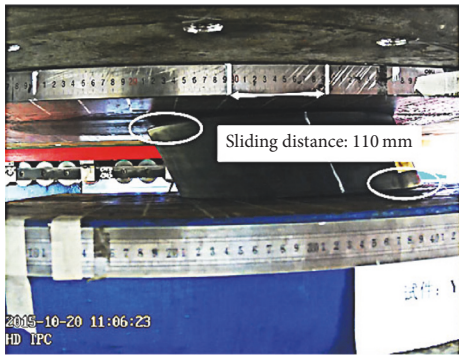

Figure 6: Specimen Y2-8/30-UB subjected to 250% ESS.

appeared as an "S" shape and showed an obvious stiffening portion. The points where the stiffening was regarded as becoming initiated were marked with blue hollow circular markers. When compared with the U-SLEBs, the different responses of the B-SLEBs could be typically characterized as a stiffening of the loading phase (C-A portion) and a degeneration of the unloading phase (A-B portion). When the ESS increased to 250%, the increasing tensile stress of the bearings was large enough to peel the rubber off the internal steel plate. It was observed that the bonded bearings bulged from the side surfaces. The bonded bearings tended to become torn if the horizontal displacement continued to increase. The horizontal force responses of the bonded bearings became obviously degenerated with the increased number of cycles. For example, with regard to specimen Y3-8/45-UB, the horizontal force degeneration value reached 62.81 kN (21.4%) during the second cycle under 250% ESS.

3.2. Horizontal Equivalent Stiffness. Figure 8(a) shows the horizontal equivalent stiffness of the type Y1 specimens plotted against the ESS with different compressive stresses.

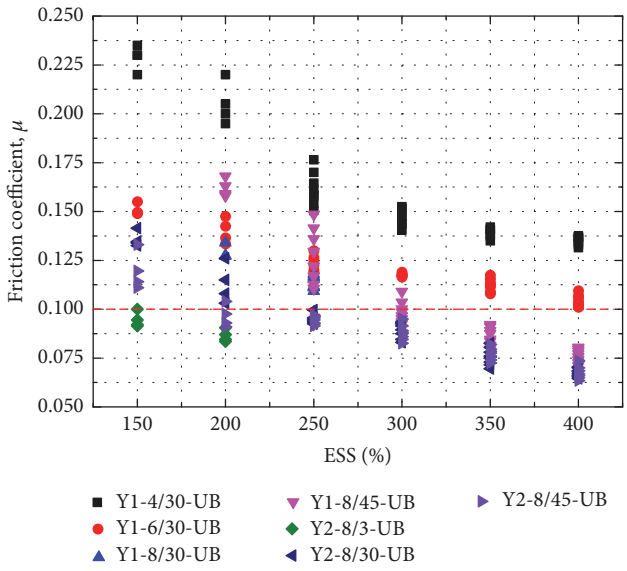

Figure 7: Observed friction versus increasing ESS.

In the figure, the solid line with square marks represents the applied compressive stress of 4 MPa. The solid line with circular marks is the applied compressive stress of 6 MPa, and the solid line with triangle marks denotes the applied compressive stress of 8 MPa. It can be observed from the figure that the horizontal equivalent stiffness decreased gradually with the increased ESS. Prior to 150% ESS, only a roll-off or slight slipping had occurred, and the degradation value of the equivalent stiffness was less than 15%. For the ESS ranging from 150% to 250%, the bearings were observed to obviously slip and a large number of rubber crumbs were found at the top and bottom surfaces of the bearings. The equivalent stiffness of specimens Y1-4/30-UB, Y1-6/30-UB, and Y1-8/30-UB was determined to decrease by 53.5%, 47.2%, and 42.2%, respectively. Then, when the ESS exceeded 250%, the degradation of the equivalent stiffness became slower. These findings also indicated that the friction behavior between the bearings and both of the supporting steel plates had basically become stable. In Figure 8(a), it can be observed that the equivalent stiffness increased with the compressive stress. When the ESS was 75%, the maximum ratio within the equivalent stiffness was 1.26 : 1.11 : 1 under the compressive stresses of 8 MPa, 6 MPa, and 4 MPa. Therefore, it could be deduced that the vertical compressive stress significantly influenced the behaviors of the U-SLEBs.

The influences of the rubber bearing types on the horizontal equivalent stiffness are shown in Figure 8(b). The horizontal equivalent stiffness of the Y1-8/45-UB and Y2-8/45-UB specimens was selected to illustrate the influences. As previously discussed, it was known that the ESS corresponding to the critical slippage of the two bearings was less than 150%. Prior to 150% ESS (Figure 8(b)), for example, when only roll-off or slight slipping had occurred, the equivalent stiffness of the natural rubber bearings was determined to be larger than that of the neoprene rubber bearings by a factor of 1.2. Both types of bearings displayed obvious slippage after reaching 150% ESS and bore different degrees of wear at the top and bottom surfaces. It can be seen that between 150% ESS and 250% ESS, the horizontal equivalent stiffness of specimens Y2-8/45-UB and Y1-8/45-UB decreased by 56.7% and 49.2%, respectively. During the slipping stage, the equivalent stiffness of the natural rubber bearings was found to be slightly less than that of the neoprene rubber bearings, which resulted in the natural rubber material becoming more obviously worn. However, the discrepancy was determined to be small.

Figure 8(c) includes the horizontal equivalent stiffness and ESS curves for the different loading rates. Overall, the equivalent stiffness increased with the loading rates, especially prior to the obvious sliding. The ratio of the equivalent stiffness under the 45 mm/s, 30 mm/s, and 3 mm/s loading rates at 75% ESS was 1.28 : 1.15 : 1. Therefore, it was concluded that the loading rates affected the initial stiffness. The equivalent stiffness and strength of the laminated elastomeric bearings were underestimated by the pseudostatic loading experiments. In the cases of sliding, the larger loading rates resulted in more serious bearing wear, as well as more rapid degeneration of the equivalent stiffness and horizontal force. However, the bearing wear mainly occurred in the preliminary stage of the sliding. The friction behaviors were found to become stable after reaching 250% ESS. The equivalent stiffnesses under the cases of 45 mm/s and 30 mm/s were observed to be relatively close.

3.3. Energy Dissipated. The area of the hysteresis loop was calculated to reflect the energy dissipation at which the test was performed [14]. The energy dissipated per cycle (EDC) under the different values of the compressive stress is plotted in Figure 9(a). It can be observed in the figure that the EDC was approximately equal for the different values of the compressive stress prior to the loading to 150% ESS. These findings can be explained by the fact that the main bearing deformation mainly included the pure elastic shear strain of the rubber layer and roll-off and all of the bearings performed at near linear elasticity. When the ESS was larger than 150%, it was observed that the EDC increased with the increasing ESS. This was found to be due to the obvious sliding of the bearings under large shear strain. The larger compressive stress led to a larger EDC value. The ratio of the EDC at 250% ESS under the compressive stresses of 8 MPa, 6 MPa, and 4 MPa was 1.25 : 1.13 : 1. Overall, there was an increase in the EDC with the increased compressive stress for all of the bearing tests.

Figure 9(b) shows the EDC and ESS curves for the different rubber materials. For the ESS of less than 150%, there was no discernible sliding found. The EDC of the natural rubber bearings was larger than that of the neoprene rubber bearings by a factor of 1.9 at 150% ESS. Meanwhile, the EDC of the two types of bearings was approximately equal after the sliding occurred and significantly larger than the value prior to the sliding stage. Therefore, it was concluded that the energy dissipation of the bearings was mainly reflected in the friction sliding.

Figure 9(c) shows the EDC and ESS curves under the different loading rates. It can be seen from the figure that the

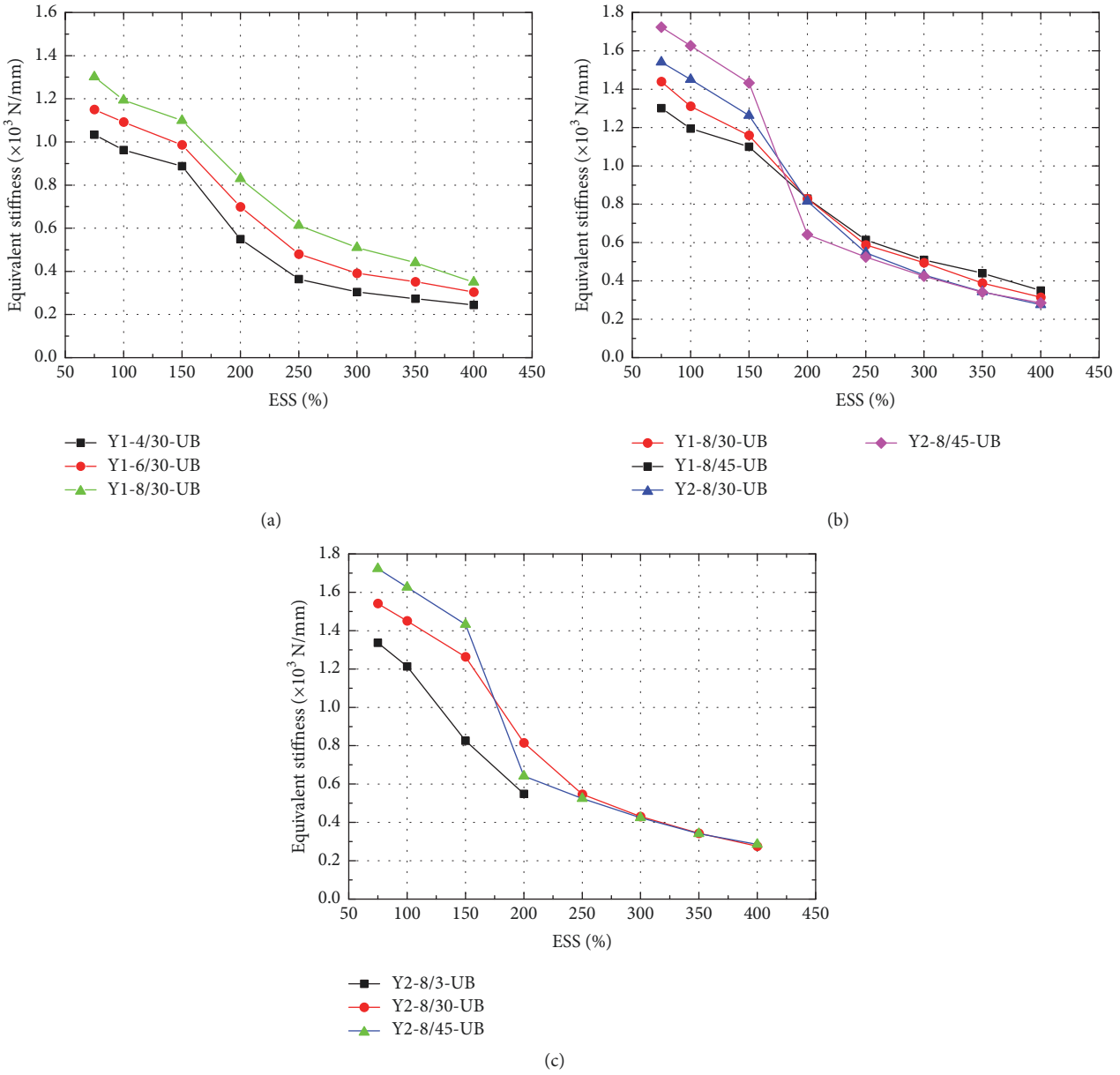

FIGURE 8: Observed equivalent stiffness versus ESS: (a) different vertical stresses; (b) different rubber materials; (c) different loading rates.

EDC obviously increased with the increasing ESS, especially after the sliding of the bearings. The EDC at 400% ESS was found to be ten times greater than that at 75% ESS. These results indicated that the energy dissipation was almost achieved during the sliding of the bearings. As illustrated by the curves in Figure 9(c), it was observed that the energy that was dissipated per cycle was independent of the loading rates.

Table 3 presents the equivalent damping ratio at different ESS values. It can be seen that, with the increase of ESS values, the equivalent damping ratio increases gradually. Especially after obvious sliding of the bearings, the equivalent damping ratio increases significantly, which indicates that the energy dissipation capacity of the bearings becomes greater.

3.4. Mechanical Properties of the Laminated Elastomeric Bearings

(1) U-SLEBs. The Coulomb friction model is the most well-known method used for considering the friction sliding characteristics after bearing sliding [19, 20]. However, with regard to the contact properties between two bodies, a transition occurs from static friction to kinetic friction, and the static frictional force has been determined to be generally larger than the kinetic frictional force. In their shear and friction experimental studies, Filipov et al. [21] established an analytical model with a sudden drop process in order to consider the transition characteristics. However, in the cases of elastomeric bearings resting on concrete or steel and subjected to horizontal forces, the adhesive friction and

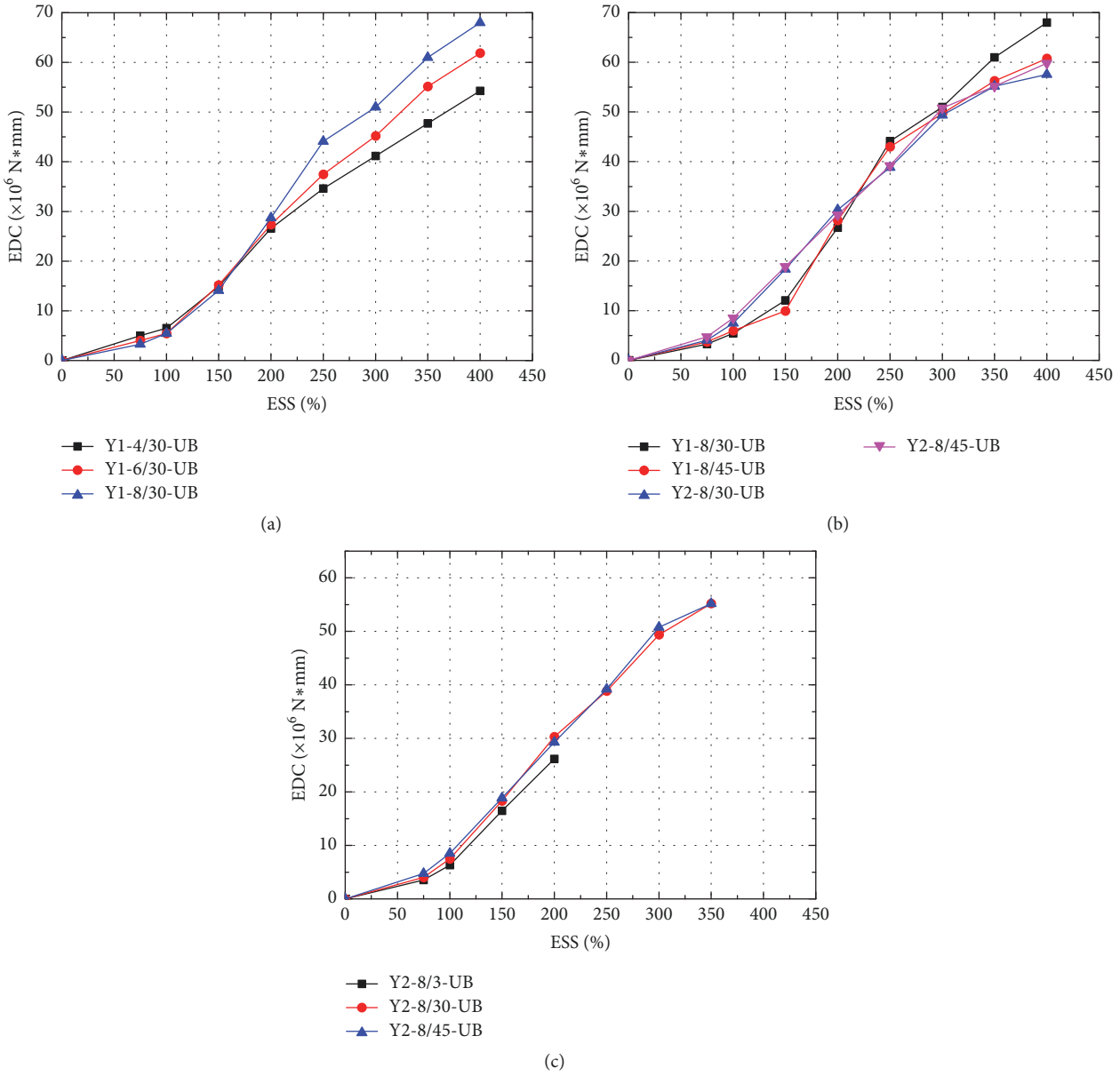

Figure 9: EDC for cyclic test: (a) different vertical stresses; (b) different rubber materials; (c) different loading rates.

Table 3: Equivalent damping ratio.

Test specimen	75% ESS	100% ESS	150% ESS	200% ESS	250% ESS	300% ESS	350% ESS	400% ESS
Y1-4/30-UB	0.158	0.167	0.236	0.301	0.367	0.404	0.421	0.440
Y1-6/30-UB	0.159	0.164	0.240	0.323	0.383	0.410	0.411	0.434
Y1-8/30-UB	0.150	0.156	0.240	0.330	0.386	0.418	0.430	0.436
Y1-8/45-UB	0.156	0.160	0.244	0.340	0.396	0.422	0.438	0.446
Y2-8/3-UB	0.154	0.157	0.287	0.381	—	—	—	—
Y2-8/30-UB	0.155	0.158	0.271	0.366	0.397	0.428	0.438	0.441
Y2-8/45-UB	0.161	0.166	0.281	0.371	0.412	0.440	0.443	0.452

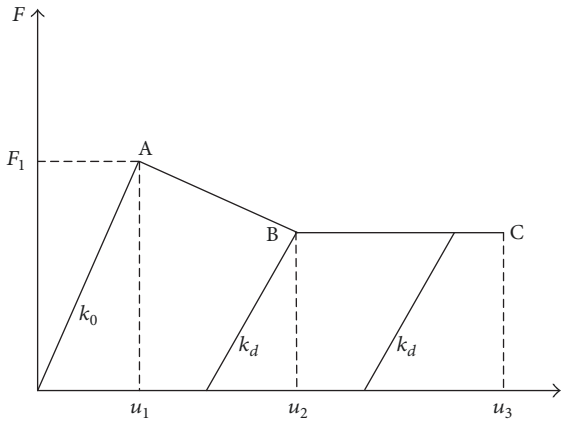

Figure 10: Mechanical model of U-SLEBs considering degradation.

traction forces tend to form at the supporting surfaces. This causes the processes of bearing friction sliding damage to be gradual rather than developing into a sudden drop process [22]. In this study, based on the horizontal force-displacement skeleton curves that are illustrated in Figures 5(a)–5(c), a mechanical model that considered the degradation was built to simulate the responses of the U-SLEBs (Figure 10). Points A and B in the figure are the key points of the mechanical model. Point A represents the initial sliding, where the corresponding displacement u_1 is equal to the ratio between the maximum static frictional force F_1 and initial stiffness k_0. Due to the wearing of the rubber becoming stable after obvious sliding, it was found that the friction behavior between the bearings and the supporting steel plates remained nearly constant. Therefore, a platform starting from Point B was used to simulate the characteristics. The corresponding displacement u_2 of Point B could be obtained from the experimental results. According to this study's experimental results, it was suggested that the displacement equaled the displacement value corresponding to 250% ESS. If there was no specific test, then the horizontal force of Point B could be 70% F_1, which was obtained through the experimental results in this study. In order to simulate the mechanical properties of the U-SLEBs using *OpenSees* software, an analytical model with two parallel nonlinear springs was developed, as shown in Figure 11. In the model, the nonlinear spring on the left side was assigned a hysteretic property to simulate the behavior of the platform. The experimental results of specimen Y2-8/45-UB were selected to verify the analytical model containing two parallel nonlinear springs. According to the skeleton curve, the values of key points A and B were 90.66 mm and 118.01 kN and 177.20 mm and 82.22 kN, respectively. An identical loading path was applied on the analytical model. Figure 12 details the comparison of hysteretic curves between the analytical and experimental results. A comparison of both the equivalent stiffness and damping ratio of specimen Y2-8/45-UB is listed in Table 4. The maximum differences of equivalent stiffness and equivalent damping ratio are 24.5% and 18.8%, respectively. However, the difference becomes smaller during the obvious sliding phase. Overall, the analytical model with two parallel nonlinear springs which had been developed using *OpenSees* software was able to correctly simulate the behaviors of the U-SLEBs.

(2) B-SLEBs. As previously mentioned, the behaviors of the B-SLEBs at large displacement demands included the bearings exhibiting strong nonlinear stiffening behaviors due to the bond boundary conditions. The hysteresis properties of the B-SLEBs were composed of three parts as follows: the A-B portion (describing the degeneration of unloading), the B-C portion (an approximately constant stiffness stage), and the C-A portion (a stiffening stage of the loading) (Figure 5(d)). In this study, a double broken line (C-D-A portion) was used to describe the stiffening stage of the loading (Figure 13). An analytical model with two parallel nonlinear springs was also developed to simulate the realistic behaviors of the B-SLEBs using *OpenSees* software (Figure 14). The nonlinear spring on the left side could be obtained using *Steel 01* material, where K_e was the initial stiffness and K_p was equal to the stiffness of the B-C portion. The double broken model on the right side could be modeled by *hysteretic* material. The recommended analytical model of the B-SLEBs was also verified through a comparison of the analytical results with the experimental results of specimen Y3-8/45-BB. Figure 15 details the comparison of hysteretic curves between the analytical and experimental results. The comparison of both the equivalent stiffness and damping ratio of specimen Y3-8/45-BB is listed in Table 5. The maximum differences of equivalent stiffness and equivalent damping ratio are 11.2% and 8.0%, respectively. It can be concluded that the analytical model with two parallel nonlinear springs which had been developed using *OpenSees* software was able to accurately simulate the behaviors of the B-SLEBs.

4. Prototype Bridge Background

4.1. Bridge Geometry and Finite Element Modeling. In order to investigate the effectiveness of U-SLEBs as isolated bearings and discuss the damage mechanism of the small-to-medium spanning highway bridges using U-SLEBs, a typical prestressed concrete continuous bridge, which had been constructed at the far-fault seismic action site in China, with main spans of (3×30 m = 90 m), was selected as a prototype for the illustration. The bridge deck was constructed with four 1.67 m high concrete box girders, and its width was 13 m. Type C50 concrete was used, which was obtained from Chinese code [23]. Each box girder was supported by two bearings, as shown in Figure 16, where D_a = 162 mm and D_b = 347 mm. The bearings used in the bridge had the same dimensions and material properties as the type Y2 specimens. They were also produced by the Hengshui China Railway Construction Engineering Rubber Co., Ltd. It was calculated that the compressive stress of a single bearing was 8 MPa. A two-column pier was built with C30 concrete and used a circular section with a diameter of 1.4 m for the middle piers. These were reinforced with HRB 335 longitudinal bars at a reinforcement ratio of 1.02%. The diameters of the longitudinal bars used in the middle piers were 25 mm. Circular stirrups with diameters of 10 mm and a pitch of 100 mm were used for all of the piers at a stirrup ratio

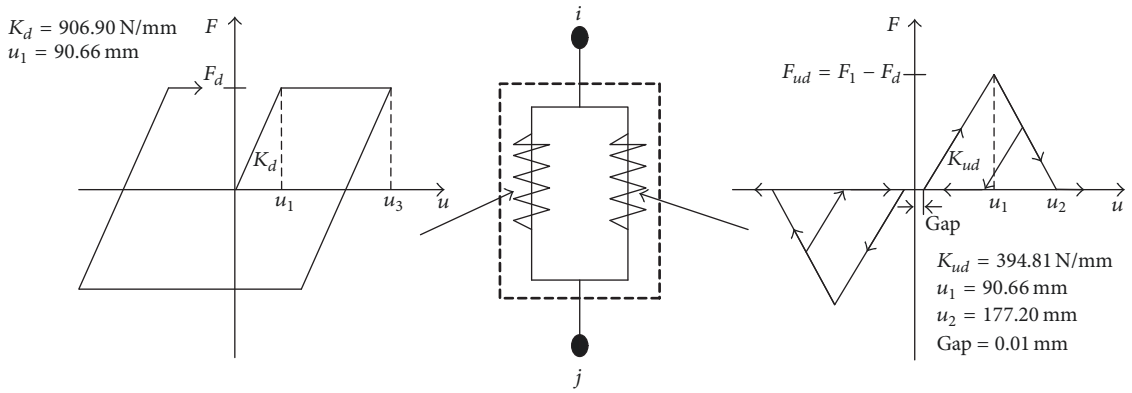

Figure 11: Analytical models of U-SLEBs.

Table 4: Comparison of both the equivalent stiffness and damping ratio of specimen Y2-8/45-UB.

ESS (%)	Equivalent stiffness			Equivalent damping ratio		
	Experiment ($\times 10^3$ N∗mm)	OpenSees ($\times 10^3$ N∗mm)	Difference (%)	Experiment ($\times 10^3$ N∗mm)	OpenSees ($\times 10^3$ N∗mm)	Difference (%)
75	1.723	1.301	24.5	0.161	—	—
100	1.627	1.301	20.0	0.166	—	—
150	1.433	1.163	18.8	0.281	0.230	18.8
200	0.641	0.706	−10.0	0.371	0.320	13.7
250	0.524	0.472	9.9	0.412	0.370	10.2
300	0.424	0.393	7.3	0.440	0.460	−4.6
350	0.341	0.336	1.3	0.443	0.477	−7.6
400	0.286	0.294	−3.0	0.452	0.495	−9.5

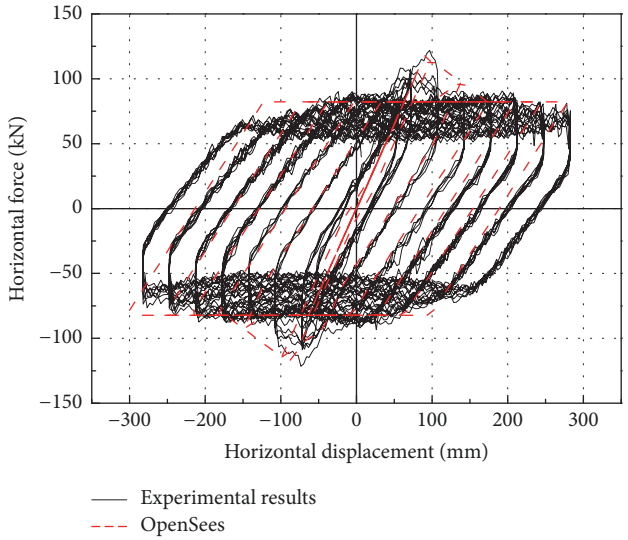

Figure 12: Comparison between experimental results and analytical results of specimen Y2-8/45-UB.

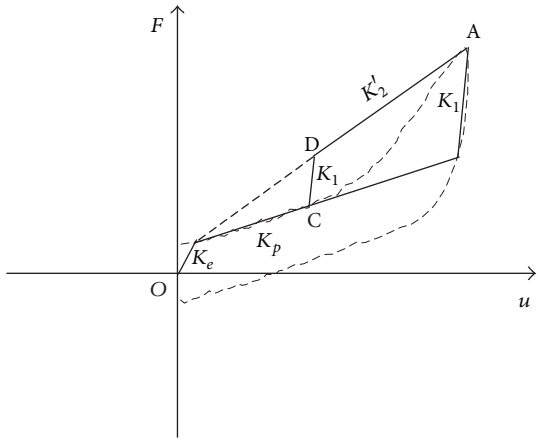

Figure 13: Nonlinear stiffening behavior of B-SLEBs.

of 0.47%, with a concrete cover thickness of 50 mm. The calculated heights of the piers were all 8 m. At the end of the pier cap, concrete shear keys were used in the transverse direction to restrict the displacement of the girder. The detailed dimensions and reinforcement layout of the shear keys are shown in Figure 16. There were 18 inverted U-shaped HRB335 rebars with diameters of 16 mm along the length direction, which extended to the pier cap of 0.56 m. Stirrups with diameters of 10 mm and a pitch of 100 mm were used for the shear keys. The initial gap between the shear keys and the girder was 0.05 m. All of the calculation values of the used material, along with the cross section, were consulted using

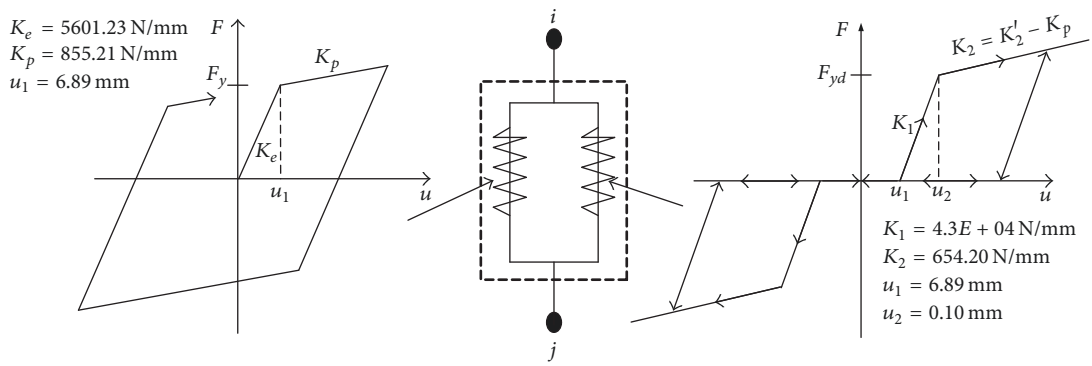

Figure 14: Analytical models of B-SLEBs.

Table 5: Comparison of both the equivalent stiffness and damping ratio of specimen Y3-8/45-BB.

ESS (%)	Equivalent stiffness			Equivalent damping ratio		
	Experiment ($\times 10^3$ N∗mm)	OpenSees ($\times 10^3$ N∗mm)	Difference (%)	Experiment ($\times 10^3$ N∗mm)	OpenSees ($\times 10^3$ N∗mm)	Difference (%)
75	1.808	1.937	−7.1	0.198	0.186	6.1
100	1.736	1.876	−8.0	0.164	0.150	8.0
150	1.656	1.842	−11.2	0.128	0.137	−7.0
200	1.636	1.748	−6.8	0.105	0.111	−5.9
250	1.585	1.641	−3.5	0.107	0.100	6.8

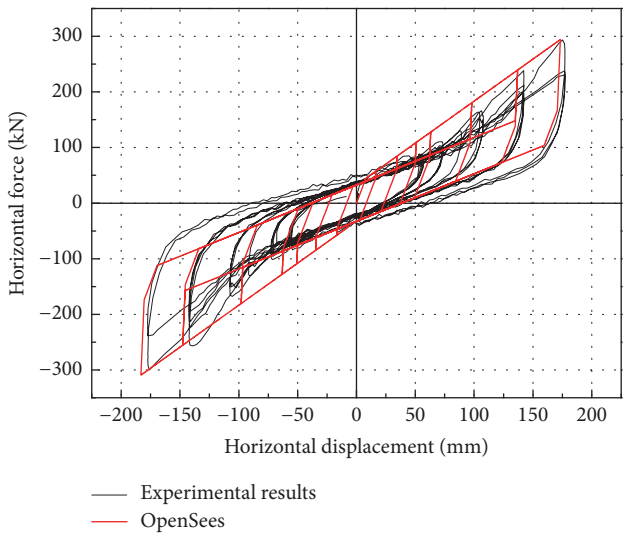

Figure 15: Comparison between experimental results and analytical results of specimen Y3-8/45-BB.

the Chinese code [23]. The bridge site belonged to type II, and the earthquake fortification was VII [17].

In order to facilitate a comprehensive analytical study, a detailed nonlinear 3D finite model was developed using *OpenSees* software. Since the girders and pier cap beams were not expected to be damaged under an earthquake, a linear elastic beam-column element was used. For two-column piers, the seismic damage usually occurs at the top and bottom of the pier, which tends to form a plastic hinge. A nonlinear fiber beam-column element was used to model the piers. The circular section of the piers was divided into three parts consisting of confined concrete fibers, unconfined concrete fibers, and longitudinal reinforcement fibers. The column and fiber cross section properties matched within 10% of each other [24]. The confined concrete and unconfined concrete fibers were modeled using *Concrete01*, which followed the Kent-Scott-Park model. *Steel02*, which followed the Giuffré-Menegotto-Pinto model, was used to define the properties of the reinforcement fibers.

The pounding effects between the girders and shear keys may cause the shear keys to become damaged or even lead to the shear keys failure, loss of function, and movement limitations. Therefore, it is necessary to take the mechanical degradation of the shear keys into consideration. In previous studies, the damage mechanism for the shear keys has been analyzed by separating the contribution of the concrete and steel skeleton in order to clearly consider the degradation of the shear keys [25, 26]. In this research study, an analytical model consisting of two hysteretic elements was developed in *OpenSees*, which could consider the contribution of the concrete and steel (Figure 17(b)). Then the pounding effects could be simulated by using a series connection of the analytical model of the shear keys and a gap element [27, 28]. The key parameters of the shear keys could be calculated according to the realistic geometric sizes and material (Table 6). The analytical models introduced in Section 3.4 were used for the laminated elastomeric bearings. The analytical model of the prototype bridge is shown in Figure 17. Also, the pile-soil interaction was not calculated in this study.

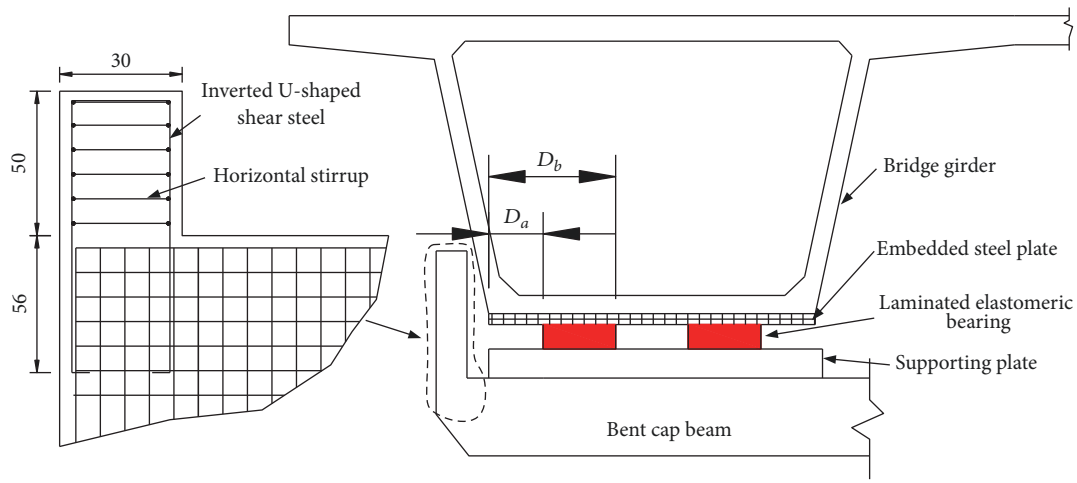

Figure 16: Details of arrangement of laminated elastomeric bearings and layout of shear key (unit: cm).

Table 6: Key parameters of the shear keys.

Performance points	A	B	C	D
Strength, V (kN)	635.13	1068.98	577.44	0
Displacement, Δ (mm)	1.3	13.4	53.3	117.7
Contribution of concrete, $V_p{}^c$ (kN)		491.54		
Contribution of steel, $V_p{}^s$ (kN)		577.44		

Four comparative analysis cases were established in this study in order to analyze the effects of the bearings with different boundary conditions on the seismic responses of the bridges, as well as to further investigate the advantages of the U-SLEBs as fuse elements to be used in small-to-medium spanning highway bridges and to formulate a reasonable design method. The cases were as follows.

Case 1. An analysis model of the bridge using U-SLEBs was developed with consideration given to the degradation of the mechanical properties of the U-SLEBs. However, the shear keys were not set up in the transverse direction.

Case 2. An analysis model of the bridge using U-SLEBs was developed with consideration given to the degradation of the mechanical properties of the both the U-SLEBs and the shear keys.

Case 3. An analysis model of the bridge using B-SLEBs was developed. However, the shear keys were not set up in the transverse direction.

Case 4. An analysis model of the bridge using B-SLEBs was developed with consideration given to the degradation of the mechanical properties of the shear keys.

4.2. Ground Motion Selection and Input. First, the target spectrum was calculated according to the type of bridge site and the earthquake fortification intensity [17]. Then, four of the actual ground motions were selected from the database of the Pacific Earthquake Engineering Research (PEER) Center, and three artificial seismic excitations were synthesized using *SeismoArtif* program. The response spectrums of the seven ground motions, as well as the mean and target spectrums, are shown in Figure 18. It can be observed from the figure that the spectrums of the analytical ground motions matched well with the target spectrum. The peak ground acceleration (PGA) values of the seven ground motions were scaled from 0.1 g to 0.7 g, at an incremental level of 0.1 g, and were input along the transverse direction. Due to the fact that the prototype bridge had been constructed at the far-fault seismic action site, the effect of the vertical seismic excitation was so small that it was neglected in this study. The average value of the calculated analytical results from the seven seismic excitations was used in this study's discussion.

5. Result Analyses and Discussion

5.1. Seismic Responses of the Different Types of Bearings. Figure 19 depicts the maximum displacements of the bearings under the different levels of ground motion. The dashed line of u_a = 252.66 mm indicates that the U-SLEBs began to slide out of the bottom plate of the girder, and a partial unseating phenomenon had occurred. Once the sliding distance exceeded the value of u_b = 437.66 mm, the U-SLEBs became completely unseated and lost the function of isolation. Since there was no restriction observed in the transverse direction, the maximum displacements of the bearings in Case 1 were determined to be larger than those of the other cases. When the PGA was 0.4 g, the maximum displacements were 217 mm or equivalent to 310% ESS. According to the

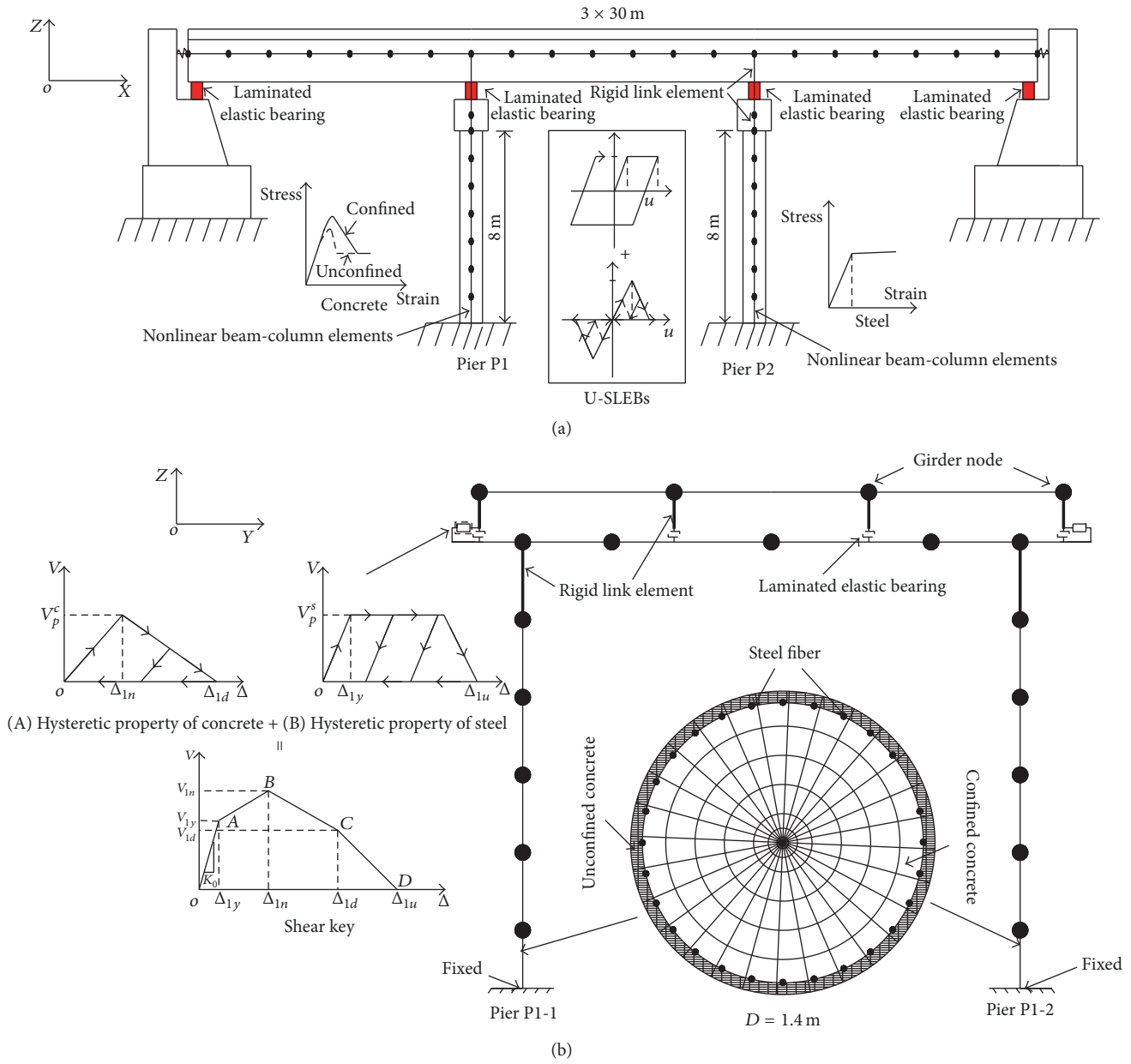

Figure 17: Finite element models of the prototype bridge: (a) elevation view; (b) bent elevation at pier P1.

testing results, this meant that the bearings in Case 1 had experienced noticeable friction sliding and had some degrees of mechanical degradation. As the PGA increased to 0.6 g, the maximum displacements reached 535 mm, and complete unseating had occurred. With regard to the bearings in Case 3, the bonded boundary conditions were applied, and there was no damage observed in the bearings when the PGA was less than 0.5 g. As the PGA reached 0.5 g and the ESS exceeded 150%, the B-SLEBs exhibited strong stiffening behaviors. Furthermore, when the ESS reached 252.8% at a PGA of 0.7 g, the bearings were torn according to the testing results' description. The damaged bearings had to be replaced, and the replacement process was complex. When the shear keys were set up in the transverse direction (such as in Cases 2 and 4), all of the bearings incurred small deformations at the PGA less than 0.5 g. The U-SLEBs in Case 2 displayed no obvious sliding, and the B-SLEBs in Case 4 also maintained normal working conditions. When the PGA reached 0.5 g, the shear keys in Case 2 were damaged, and the capacity of movement limitation was completely lost. This led to a major increase in the bearing displacements. The U-SLEBs experienced obvious friction sliding, as well as near complete unseating, when the PGA was 0.6 g. The B-SLEBs in Case 4 had no damage occurrence due to the movement limitation of the shear keys in the transverse direction. As previously discussed, the U-SLEBs were found to easily slide under the seismic excitations, and the primary seismic damage of the U-SLEBs was friction sliding and unseating. This was found

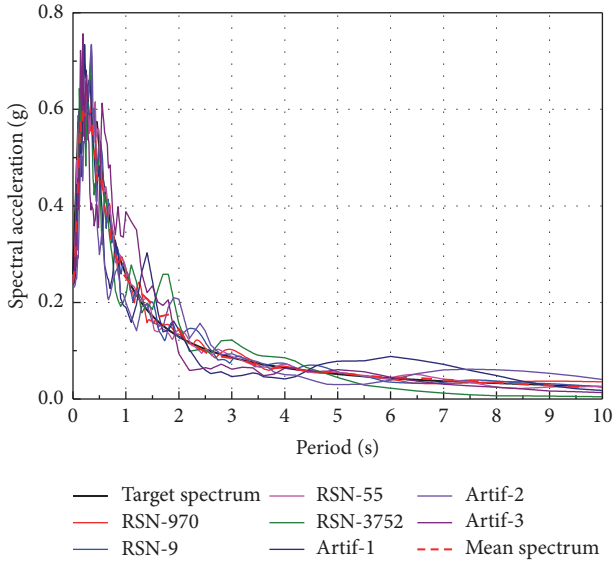

Figure 18: Target spectrum and the spectrum of selected ground motions.

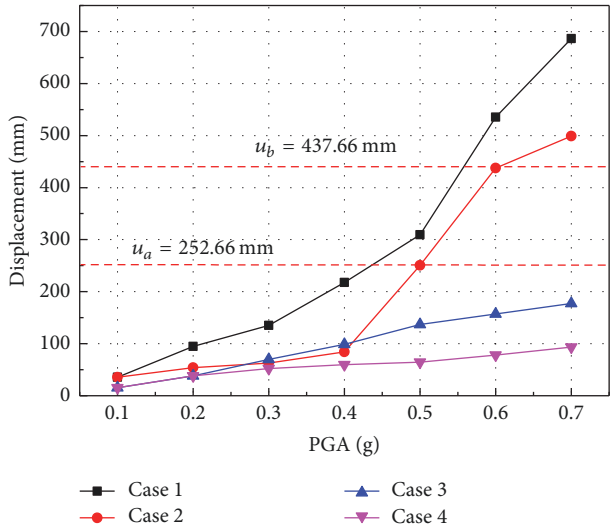

Figure 19: Maximum displacements of laminated elastomeric bearings.

to be in agreement with the recorded seismic damage of the small-to-medium spanning highway bridges in recent years. While the B-SLEBs exhibited stiffening behaviors, the main seismic damage of the B-SLEBs resulted from tearing. At the same time, its replacement processes are complicated, and the costs are high. It is recommended that the shear keys should be constructed with reasonable designs in the transverse direction, which was found to effectively reduce the damage to the bearings.

5.2. Effects on the Displacements of the Girders. The displacement responses of the girders are directly related to the seismic responses of the isolation bearings, pounding effects, and earthquake intensities. Figure 20 shows the maximum

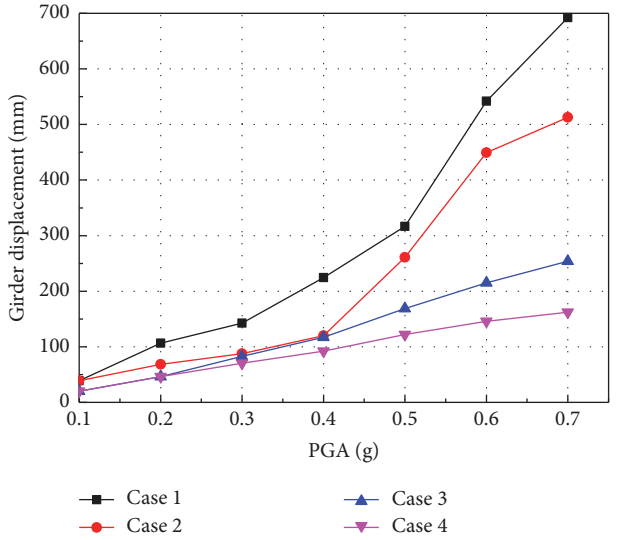

Figure 20: Maximum girder displacements.

displacement values of the girders under the different levels of ground motion. It can be seen that the maximum displacement obviously increased with the increases in the PGA. However, the growth rates were different due to the boundary conditions of the bearings and the movement limitations of the shear keys. The maximum displacement values of the girder in Case 1 had the largest increase, since there were no shear keys to restrict the girder's movement. While the bearings in Case 3 had a bonded application, the displacement of the girder had been certainly limited by the B-SLEBs due to the fact that sliding was prevented. The value was found to be less than that of Case 1. The shear keys in the transverse direction can potentially play a significant role in girder movement limitations. For example, in Case 2, when the PGA was less than 0.5 g, the girder displacement was greatly limited, and the maximum displacement value was 120 mm. However, the shear keys were completely damaged, and a loss of movement limitation resulted when the PGA reached 0.5 g (Figure 21). This led the girder's displacement to dramatically increase. Since girder movement was constrained by the B-SLEBs and shear keys in Case 4, it only displayed slight displacement. Therefore, it was concluded that a bridge using U-SLEBs will have larger girder displacement than a bridge using B-SLEBs. It was observed that when the PGA reached 0.5 g in this study, the difference was more than twice the amount.

5.3. Effects on the Damage of the Piers. The equivalent yield curvature of the piers' bottom section was $2.04E-03\,\mathrm{m}^{-1}$, which was determined by analyzing the moment-curvature on the fiber section developed in Section 4.1. Figure 22 details the curvature variations of the pier's bottom section under the different levels of ground motion. It was observed that the curvature increased with the PGA, which indicated that the damage status of the pier was being gradually aggravated. Since an unbonded application was used in Case 1, the seismic force transferred to the substructure was greatly isolated,

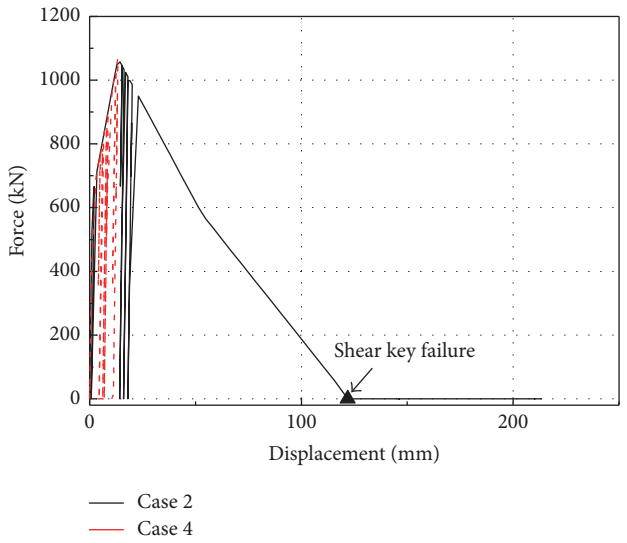

Figure 21: Force-displacement curves of the shear key under PGA = 0.5 g.

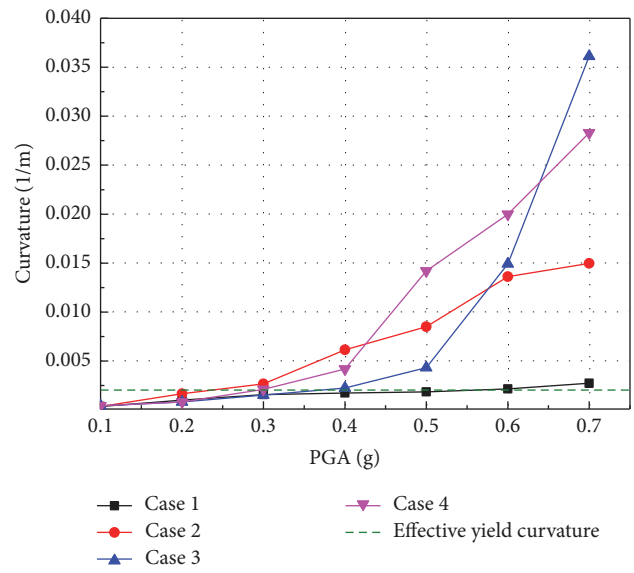

Figure 22: Maximum curvature of pier bottom section under different level ground motions.

which led to the curvature value in Case 1 being basically less than that of Case 3. This effectively mitigated the damage of the substructure. However, the B-SLEBs used in Case 3 displayed stiffening behaviors after the PGA reached 0.5 g and thereby increased the seismic demands of the piers. The shear keys in the transverse direction were able to effectively limit girder movement. However, the pounding between the shear keys and girder increased the seismic force transferred to the piers. Therefore, the curvature of the pier's bottom section in Case 2 was found to be larger than in the other cases when the PGA was less than 0.5 g and the pier had yielded at a PGA of 0.3 g. A pounding phenomenon also occurred in Case 4. However, its effect was significantly reduced due to the movements of the girder being limited by the B-SLEBs. When the PGA reached 0.5 g, the increase of the pounding effect was large enough to raise the seismic demand of the pier and exceeded the curvature value of Case 2. Overall, the curvatures of the cases without shear keys were less than those of the corresponding cases which had shear keys set up in the transverse direction. These results indicated that the shear keys had significant effects on the transmission of the seismic force of superstructures.

5.4. Discussion of the Damage Mechanism of the Prototype Bridge in the Transverse Direction. It could be concluded from the above stated results that the U-SLEBs have the ability to perform good isolation for providing stable friction sliding, such as in Case 1, where its substructure suffered the smallest earthquake event. However, the superstructure displayed the largest displacements, which would potentially lead to serious damage of the girder falling occurrence. Therefore, it would be necessary to set up shear keys to limit the displacements, such as in Case 2, which represents the most common type of small-to-medium spanning highway bridges in China. When the PGA of the seismic excitations was small (less than 0.2 g in this study), only shear deformations occurred. The isolation function had not yet begun to work effectively. As the PGA increased (ranging from 0.2 g to 0.4 g in this study), the shear deformations of bearings became large enough that friction sliding also occurred, thus resulting in pounding between the shear keys and girder. When the PGA became larger (reaching 0.5 g in this study), the shear keys underwent complete damage. The completely damaged shear keys could no longer restrict the displacements of the girder and bearings. Meanwhile, the U-SLEBs displayed a certain degree of degradation due to the obvious friction sliding and even suffered complete unseating. However, this response process was able to isolate the inertia force of the superstructure and mitigate the damage to the pier. A slightly damaged pier can recover by using temporary reinforcement measures, such as in the case of the Shoujiang Bridge detailed in Figure 1(b). The seismic damage that occurred in Case 2 clearly explained the seismic damage investigations of small-to-medium spanning highway bridges in China. With regard to Case 3, the bearings were unable to slide for a bonded application. This could potentially restrict the displacement of the superstructure to some extent. Nonetheless, it increased the damage occurrence in the bearings and substructure. Similarly, although the shear keys were set up in the transverse direction in Case 4, the damage positions of the bridge system were transferred to the potential plastic hinge area within the substructure, which usually tends to cause serious damage to piers and piles, as evidenced by the Baihua Bridge detailed in Figure 1(a).

In this research study, based on the aforementioned discussion and the seismic damage investigation, it was found that the bridges using U-SLEBs displayed good seismic performances. However, the strength and initial gaps of the shear keys should be elaborately designed in order to achieve a balance between the isolation efficiency and the girder displacements. Also, their constructions were both convenient and

economical. Although the bridges using B-SLEBs displayed good performances in controlling girder displacements, the bearings and substructures showed greater risks of damage, especially in the western areas with high seismicity. Once the bearings become torn and the substructures are severely damaged, then the earthquake relief and postdisaster reconstructions will be affected. Therefore, it can be confirmed that, for small-to-medium spanning highway bridges using laminated elastomeric bearings without any anchoring, effective seismic isolations could be performed with low costs. The residual displacement of the girders due to the bearing sliding can be repaired by an incremental launching method, which is a simple operation. This is faster and more economical than repairing the seismic damage of the substructure.

6. Conclusions

This study first compared the behavioral characteristics between the U-SLEBs and B-SLEBs through a series of cyclic loading experiments. Then, analytical models for the U-SLEBs and B-SLEBs were proposed and verified based on the experimental results. The effects of the different types of bearings during the seismic excitations were investigated by examining the seismic responses of a typical prestressed concrete continuous bridge. The comparative analyses led to the following conclusions.

(1) The deformation of U-SLEBs can be divided into three states: pure elastic shear strain of rubber layer, roll-off at the top and bottom surfaces of the bearing, and obvious friction sliding. The U-SLEBs could display stable hysteretic behavior, even after suffering multiple reversed cycles of large displacements. Although the bearings were found to have a certain degree of degradation from obvious friction sliding, this did not result in bearing failures. Therefore, the U-SLEBs could potentially play the role of seismic isolation prior to unseating. The typical hysteretic loop of the U-SLEBs under a fully reversed cyclic loading can be approximated in portion with the constant stiffness stage, in portion with the stiffening stage of the loading, and in portion with the degeneration of the unloading. The B-SLEBs exhibited strong nonlinear stiffening behaviors under the large displacement demands. Also, the bearing capacity of displacement was found to be limited. When a certain shear deformation was achieved, a force degradation occurred, and the bearings were torn.

(2) The horizontal equivalent stiffness and the EDC of the U-SLEBs were found to increase with the increases in the compressive stress. However, the larger compressive stress led to smaller friction coefficients. As the loading rate increased, the horizontal equivalent stiffness of the U-SLEBs became larger. This was found to not have a significant effect on the energy dissipation. Meanwhile, the increased loading rate led to the formation of high temperatures between the bearings and the supporting surfaces and resulted in increases in the friction coefficient. The energy dissipation of the bearings was mainly reflected in the friction sliding. The equivalent damping ratio increases gradually with ESS.

(3) The analytical model of the U-SLEBs developed in this paper was able to correctly consider the mechanical degradation due to obvious friction sliding. The results of different comparison models show that bridges using U-SLEBs should set up shear keys in the transverse direction. Otherwise, the bearing displacement cannot be limited and may cause girder falling. The U-SLEBs and shear keys can be designed as sacrificial components for the bridge systems. They will be damaged first during seismic excitations, which can effectively mitigate the damage to the substructures. This bridge design method, which has been adopted in small-to-medium spanning highway bridges in China, has exhibited superior seismic performance during recent earthquake events.

(4) The analytical model of the B-SLEBs developed in this study was able to simulate realistic behaviors under seismic excitations. Although bridges using B-SLEBs have displayed better performances in girder movement limitations, the bearings may become torn, and the damage has been found to mainly occur in the piers. The repair processes for the damaged components are complicated, and the costs are high, which is not conducive to earthquake relief and postdisaster reconstructions.

Conflicts of Interest

The authors declare that there are no conflicts of interest regarding the publication of this paper.

Acknowledgments

The research presented herein was supported by the Project of China International Science and Technology Cooperation (Grant no. 2009DFA82480) and Science and Technology Project of Communications' Construction in Western China, MOC (Grant no. 2009318223094).

References

[1] J. Li, T. Peng, and Y. Xu, "Damage investigation of girder bridges under the Wenchuan earthquake and corresponding seismic design recommendations," *Earthquake Engineering and Engineering Vibration*, vol. 7, no. 4, pp. 337–344, 2008.

[2] H. Qiang, D. Xiuli, L. Jingbo, L. Zhongxian, L. Liyun, and Z. Jianfeng, "Seismic damage of highway bridges during the 2008 Wenchuan earthquake," *Earthquake Engineering and Engineering Vibration*, vol. 8, no. 2, pp. 263–273, 2009.

[3] K. H. Wang, H. Wei, Q. Li, and Y. Li, "Philosophies on seismic design of highway bridges of small or medium spans," *China Civil Engineering Journal*, vol. 45, no. 9, pp. 115–121, 2012.

[4] K. H. Wang, C. Li, Q. Li, and Y. Li, "Seismic design method of small and medium span bridge considering bearing friction slipping," *Engineering Mechanics*, vol. 31, no. 6, pp. 85–92, 2014.

[5] W. L. Zhuang and L. S. Chen, *Analysis of Highways' Damage in the Wenchuan Earthquake*, China Communications Press, Beijing, China, 2013 (in Chinese).

[6] D. H. Tobias, R. E. Anderson, C. E. Hodel, W. M. Kramer, R. M. Wahab, and R. J. Chaput, "Overview of earthquake resisting system design and retrofit strategy for bridges in Illinois," *Practice Periodical on Structural Design and Construction*, vol. 13, no. 3, pp. 147–158, 2008.

[7] K. C. Chang, C. H. Lu, and K. Y. Liu, "Displacement-based design for highway bridges with function bearing system," Tech. Rep. Rep. NO. NCREE-11-015, National Center for Research on Earthquake Engineering, Taiwan, China, 2011 (Chinese).

[8] J. S. Steelman, L. A. Fahnestock, E. T. Filipov, J. M. Lafave, J. F. Hajjar, and D. A. Foutch, "Shear and friction response of nonseismic laminated elastomeric bridge bearings subject to seismic demands," *Journal of Bridge Engineering*, vol. 18, no. 7, pp. 612–623, 2013.

[9] J. S. Steelman, *Sacrificial Bearing Components for Quasi-Isolated Response of Bridges Subject to High-Magnitude, Low-Probability Seismic Hazard [Doctoral, thesis]*, University of Illinois, Champaign, IL, USA, 2013.

[10] J. McDonald, E. Heymsfleld, and R. R. Avent, "Slippage of neoprene bridge bearings," *Journal of Bridge Engineering*, vol. 5, no. 3, pp. 216–223, 2000.

[11] N. L. Xiang, X. X. Cui, and J. Z. LI, "Experimental study on sliding friction behavior of laminated rubber bearing and its mechanical model," *Journal of Tongji University (Natural Science)*, vol. 44, no. 12, pp. 1828–1834, 2016 (Chinese).

[12] C. Li, *Performance Based Seismic Design of Small and Medium Span Girder Bridges [Doctoral, thesis]*, Southeast University, Nanjing, Jiangsu, China, 2015 (in Chinese).

[13] H. Toopchi-Nezhad, M. J. Tait, and R. G. Drysdale, "Bonded versus unbonded strip fiber reinforced elastomeric isolators: Finite element analysis," *Composite Structures*, vol. 93, no. 2, pp. 850–859, 2011.

[14] D. Konstantinidis, J. M. Kelly, and N. Makris, "Experimental investigations on the seismic response of bridge bearings," Tech. Rep. Report No. EERC 2008-02, Earthquake Engineering Research Center, College of Engineering, University of California, Berkeley, Calif, USA, 2008.

[15] SAC, *China National Standard: Rubber Bearings-Part 1: Seismic-Protection Isolators Test Methods (GB/T 20688.1-2007)*, Standardization Administration of the People's Republic of China, Beijing, China, 2007 (in Chinese).

[16] MOTC, "China Transportation Standard: Plate Type Elastomeric Pad Bearings for Highway Bridges (JT/T 4-2004)," China Ministry of Transportation and Communications Press, Beijing, China, 2004 (in Chinese).

[17] MOTC, *JTG/T*, China Ministry of Transportation and Communications Press, Beijing, China, 2008 (in Chinese).

[18] C. S. Tsai, T.-C. Chiang, B.-J. Chen, and S.-B. Lin, "An advanced analytical model for high damping rubber bearings," *Earthquake Engineering & Structural Dynamics*, vol. 32, no. 9, pp. 1373–1387, 2003.

[19] L. Y. Nie, J. Z. Li, S. D. Hu, and L. C. Fan, "Dynamic response coupled by rubber bearing sliding in interchange bridge under earthquake," *Engineering Mechanics*, vol. 23, no. 11, pp. 14–20, 2006.

[20] K. Y. Liu, K. C. Chang, and W. C. Cheng, "Seismic performance of skewed bridge with friction type rubber bearings," in *Proceedings of the 14th World Conference on Earthquake Engineering*, Beijing, China, October 2008.

[21] E. T. Filipov, L. A. Fahnestock, J. S. Steelman, J. F. Hajjar, J. M. LaFave, and D. A. Foutch, "Evaluation of quasi-isolated seismic bridge behavior using nonlinear bearing models," *Engineering Structures*, vol. 49, pp. 168–181, 2013.

[22] G. Russo and M. Pauletta, "Sliding instability of fiber-reinforced elastomeric isolators in unbonded applications," *Engineering Structures*, vol. 48, pp. 70–80, 2013.

[23] MOTC, *China transportation standard: code for design of highway reinforced concrete and prestressed concrete bridges and culverts (JTG D62-2004)*, China Ministry of Transportation and Communications Press, Beijing, China, 2004 (in Chinese).

[24] A. Aviram, K. R. Mackie, and B. Stojadinovic, "Guidelines for nonlinear analysis of bridge structures in California," Tech. Rep., Pacific Earthquake Engineering Research Center, University of California, Berkeley, Calif, USA, 2008.

[25] S. H. Megally, P. F. Silva, and F. Seible, "Seismic response of sacrificial shear keys in bridge abutments," Tech. Rep. Report No. SSRP-2001/23, Structural Systems Research Project, University of California, San Diego, Calif, USA, 2001.

[26] L. Q. Xu and J. Z. Li, "Design and experimental investigation of a new type sliding retainer and its efficacy in seismic fortification," *Engineering Mechanics*, vol. 33, no. 2, pp. 111–118, 2016 (in Chinese) (Chinese).

[27] H. Tang, J. Z. Li, and C. Y. Shao, "Seismic performance of small and medium span girder bridges with plate type elastomeric pad bearings in the transverse direction," *China Journal of Highway and Transport*, vol. 29, no. 3, pp. 55–65, 2016 (in Chinese).

[28] N. Xiang and J. Li, "Seismic performance of highway bridges with different transverse unseating-prevention devices," *Journal of Bridge Engineering*, vol. 21, no. 9, Article ID 04016045, 2016.